



A proposal improvement in flatness measurement in strip rolling

Sami Abdelkhalek^{1,2}

Received: 23 September 2017 / Accepted: 14 February 2018 / Published online: 21 February 2018
© Springer-Verlag France SAS, part of Springer Nature 2018

Abstract

In strip rolling flatness of the final product is controlled inline with a roll sensor placed at the outgoing of the tandem mill to measure the longitudinal (in the rolling direction) internal stress profile throughout the coil. This profile involves resultant force and sometimes resultant moment (due to preset anomaly for example) equilibrated by the coiler. When strip is relaxed these two quantities are eliminated and there remain residual stresses in the strip. Since negative residual stresses are the main origin of defects, operators subtract the resultant force from measurements to visualize the residual stress profile in real time and detect negative values, without considering the resultant moment. In this paper we show that to predict flatness defects correctly we have to subtract resultant moment too. Otherwise, unpredictable defects manifest in the delivered product.

Keywords Post buckling · Asymptotic numerical method · Residual stress · Flatness defect · Strip rolling

Introduction

In strip rolling a roll sensor is usually placed at the outgoing of tandem mill to measure longitudinal residual stress profile S_{xx}^{res} in strips [1]. It is placed at few meters away from the bite exit, where other stress components may be neglected, and it precedes the coiler that applies tension to the product (see Fig. 1). Buckling of the structure can happen if residual stresses remain excessively compressive and consequently undesirable flatness defects appear. The strip remains flat in-line if coiler tension is sufficiently large and full extent as well as geometric shape of defects appear when tension is unloaded. When defects are unseen by the operators inline, they are called latent defects and they become manifest if they arise in relaxed strip. Control in real time of residual stresses is performed through actuator forces (bending forces for example) in order to avoid compressive areas and ensure flat strips to deliver. When strip is stretched and looks flat defects are expected where stresses remain compressive. For this reason, latent defects are usually related to compressive residual stress measured with roll

sensors. For example, a wavy edge (manifest defect) is predicted if compressive stresses (latent defect) are located there.

In a previous study [2] authors show how latent defects turn to manifest defects during tension unloading of rolled strips. A numerical model based on finite element model using asymptotic numerical method algorithm to solve nonlinear problems is employed. It is mentioned that in some cases defects reveal surprisingly where residual stresses are measured positive which makes flatness control difficult and relationship latent-manifest defects questionable. It is the only study of flatness defect for a such intricate cases existent in literature to our knowledge, where this result is evoked but no more. The purpose of this paper is to go farther and complete works presented in [2] by deeper analysis of relation latent-manifest defects to fulfill better inline flatness mastering. This study is based on the same finite element model used in reference [2]. A representative part of coil is considered (usually mesh length is equal to four or five times the width). Simulation begins by stretching the specimen and introducing measurement values of residual stresses provided by roll sensors to reproduce in-line state of strips. Tensile unloading, which is the greatest interest of this study, is then performed to simulate the final quality of product and therefore we analyze the relation latent-manifest defects. Since roll sensor measures tensile stress repartition in strip width, conventionally resultant force is subtracted in order to acquire the residual stress profile. This work demonstrates that tensile stress could involve resultant moment which also has to be eliminated. If not, compressive

✉ Sami Abdelkhalek
sami_abdelkhalek@hotmail.com

¹ Military academy of Fondouk Jedid, 8012 Nabeul, Tunisia

² Applied Mechanics and Systems Research Laboratory, Tunisia Polytechnic School, University of Carthage, B.P. 743-2078, La Marsa, Tunisia

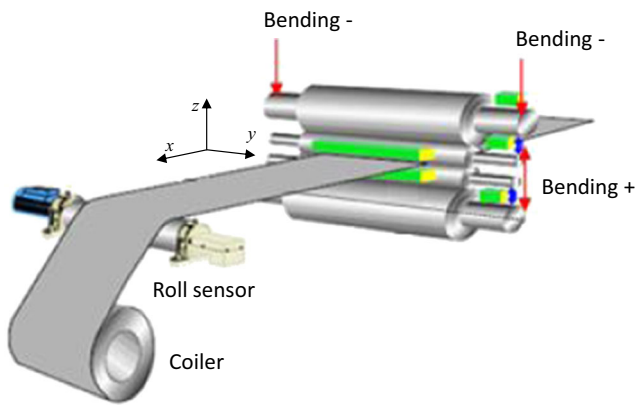


Fig. 1 Residual stress measurements using roll sensors

regions might be undetected to predict correctly flatness defects, thus relation latent-manifest is imprecise.

Numerical basis of the finite element model

In many cases flatness prediction is uncertain because residual stress measurements are complex or even with regular measurements buckling can happen with unexpected mode in relaxed strip. Hence, a precise buckling model is necessary to simulate flatness defects occurred in tensile unloading. The model used in this work has been presented previously in the reference [2]. It is a finite element model based on quadratic shell and the enhanced assumed strain formulation [2, 3]. Referring to Fig. 2 the displacement u is a composition of displacement v and rotation w of the mean surface of the shell:

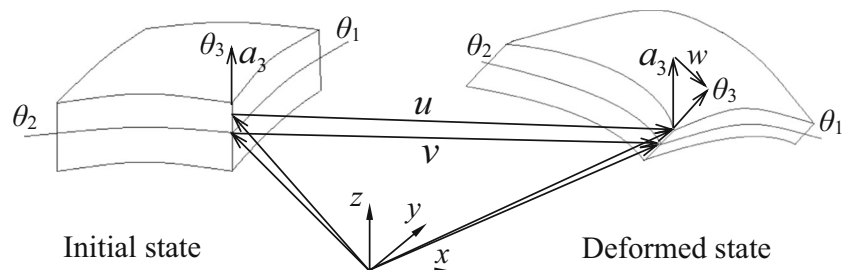
$$u(\theta_1, \theta_2, \theta_3) = v(\theta_1, \theta_2) + \theta_3 w(\theta_1, \theta_2) \tag{1}$$

where $(\theta_1, \theta_2, \theta_3)$ are the convective curvilinear coordinates.

The enhanced assumed strain concept (EAS) [3, 4] is used to improve the performance of elements: the compatible Green-Lagrange strain field γ^c is enriched by additional strain field $\tilde{\gamma}$ chosen linear through the shell thickness and orthogonal to the stress field. Consequently, the strain field γ of the shell is expressed as:

$$\begin{cases} \gamma = \gamma^c + \tilde{\gamma} \\ \int_{\Omega} S^t : \tilde{\gamma} d\Omega = 0 \end{cases} \tag{2}$$

Fig. 2 Shell formulation



where S^t is the transposition of the second Piola-Kirchhoff stress tensor S .

The mechanical problem is described in Fig. 3 and its formulation is based on the stationary condition of the Hu-Washisu functional and we consider a linear constitutive law:

$$\begin{cases} \int_{\Omega} S^t : \delta\gamma^c d\Omega = \lambda^{(P)} \int_{\partial\Omega_3} P \delta u ds \\ \int_{\Omega} S^t : \delta\tilde{\gamma} d\Omega = 0 \\ S = \mathbb{C} : (\gamma^c + \tilde{\gamma}) + \lambda^{(S)} S^{res} \end{cases} \tag{3}$$

Where \mathbb{C} is the matrix of elastic constants, δu is the virtual displacement field. Parameters $\lambda^{(P)}$ and $\lambda^{(S)}$ are scalar parameters to vary tension and residual stress levels. The parameter $\lambda^{(P)}$ varies from 0 to 1 to stretch the strip and from 1 to 0 to unload tension. $\lambda^{(S)}$ varies from 0 to 1 to introduce residual stresses in stretched state. Boundary conditions are imposed in edges $\partial\Omega_1, \partial\Omega_2, \partial\Omega_3$ and $\partial\Omega_4$ depending on problems.

The model uses the asymptotic numerical method (ANM) algorithm, a powerful tool to solve problems with instabilities. Details of the model formulation with ANM are presented in the reference [2]. The ANM consists in approximating a non-linear problem by succession of polynomial approximation as in the example in Fig. 4 (the PADE approximation is possible [5]); hence variables are expressed into series according to the power of the convergence radius a :

$$\begin{aligned} U(a) &= U_0 + aU_1 + a^2U_2\dots \\ \lambda(a) &= \lambda_0 + a\lambda_1 + a^2\lambda_2\dots \end{aligned} \tag{4}$$

Here $U = (u, \tilde{\gamma}, S)$ and λ is equal to $\lambda^{(S)}$ or $\lambda^{(P)}$.

Problem statement

When flatness defects are masked inline due to large tension, they are deduced from longitudinal residual stresses S_{xx}^{res} measured across the width direction. In practice flatness defects are expressed by I-Units (flatness index). This quantity is equivalent to a longitudinal elastic deformation developed by buckling that inducing “shrinking” of longitudinal material fibers at each position y_i , caused by $S_{xx}^{res}(y_i)$ after tension unloading (see

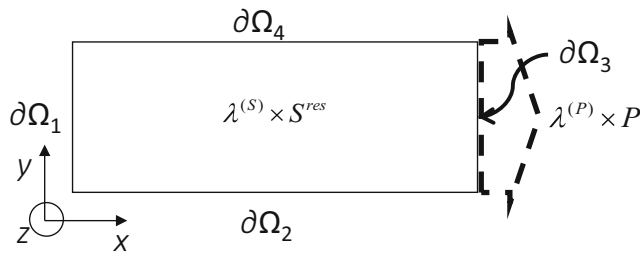


Fig. 3 Physical problem to simulate

example in Figs. 5 and 6). There are two possible representations of I-Units. Either we divide the longitudinal residual stress profile by the Young modulus \$E\$ of the strip and we use \$IU^\sigma\$ (see Fig. 5), or we use lengths of longitudinal material fibers \$\tilde{L}\$ normalized by a characteristic length \$\bar{L}\$ (Fig. 6) and we use \$IU^g\$ (a scale factor equal to \$10^5\$ is usually introduced in order to manipulate integers):

$$IU_{y_i}^\sigma = \frac{S_{xx}^{res}(y_i)}{E} 10^5 \tag{5}$$

$$IU_{y_i}^g = \frac{\tilde{L}(y_i) - \bar{L}}{\bar{L}} 10^5 \tag{6}$$

In many references \$IU^\sigma\$ and \$IU^g\$ are assumed equivalent as in [1].

Since \$\frac{\tilde{L}(y_i) - \bar{L}}{\bar{L}}\$ is positive and equivalent to longitudinal elastic deformation of the material fiber \$i\$, based on one-dimensional Hooke's law we define \$\psi(y_i)\$ as:

$$\psi(y_i) = -E \frac{\tilde{L}(y_i) - \bar{L}}{\bar{L}} \tag{7}$$

\$\psi(y_i)\$ is equivalent to a longitudinal compressive stress. We express also \$\bar{\psi}\$ as the resultant of \$\psi(y_i)\$ calculated by the relation below:

$$\bar{\psi} = \frac{1}{b} \int_b \psi(y) dy = \frac{\sum_i \psi(y_i) \Delta y_i}{b} \tag{8}$$

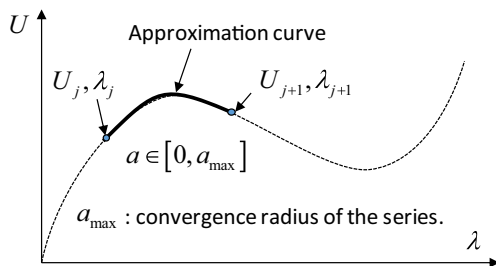


Fig. 4 The ANM technique

Longitudinal residual stress profile measurements

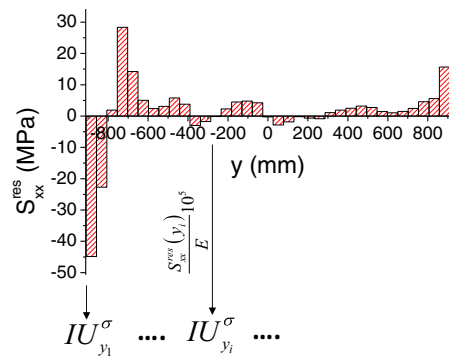


Fig. 5 Flatness index can be deduced from residual stress measurements

where \$b\$ is the strip width. Therefore, \$\psi^{res} = \psi(y_i) - \bar{\psi}\$ denotes a residual stress field deduced from geometric defects which can be also expressed as:

$$\psi^{res}(y_i) = -10^5 E \times IU_{y_i}^g - \bar{\psi} \tag{9}$$

The numerical model has to give \$\psi^{res}(y_i)\$ closer to measurements \$S_{xx}^{res}(y_i)\$. In the first test (case 1) we consider longitudinal residual stress profile measured inline presented in Fig. 7. With the numerical model we simulate the portion of the strip between the bite exit and the coiler. The bite side (\$\partial\Omega_1\$ in Fig. 3) is clamped, the coiler side (\$\partial\Omega_3\$ in Fig. 3) is simply supported and edges (\$\partial\Omega_2\$ and \$\partial\Omega_4\$ in Fig. 3) are free and we take a length equal to five times the width. This case is representative of e.g. automotive strip formats (width 1700–1800 mm). The geometric and mechanical characteristics are presented in Table 1 and the rolling tension is 40 MPa. We use \$60 \times 40\$ elements (60 in length, 40 in width). The overview of residual stress profile leads to predict a wavy center defect. Indeed, simulation gives flat strip inline and a wavy center in relaxed strip with approximately 5 mm of amplitude (see Fig. 8). The global mode

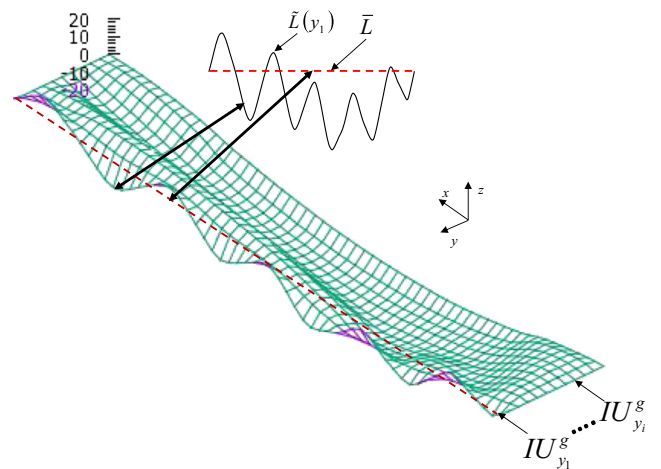


Fig. 6 Flatness index can be deduced from geometric shape of the strip. Here the edge corresponding to \$IU_{y_i}^g\$ is considered

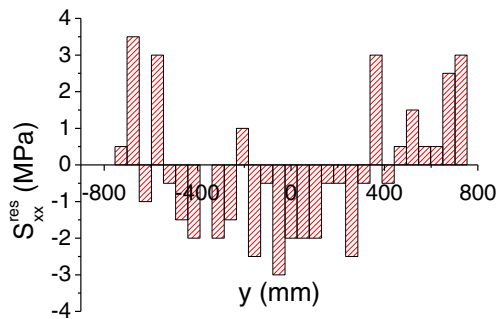


Fig. 7 Residual stress profile measured for case 1 (courtesy of Arcelormittal)

observed (amplitude approximately equal to 30 mm) is not qualified as critical flatness defect from industrial point of view since, as it is a developable defect, it is easily corrected by levelling. The post-buckling curve $\lambda^{(P)}$ function of vertical displacement u_z of a control node in the center of the structure is plotted in Fig. 9. This figure shows complex pathway in tensile unloading where we note the first bifurcation point at $\lambda^{(P)}$ equal to 0.0425 and other limit and quasi-bifurcation points. The comparison between ψ^{res} and S_{xx}^{res} in Fig. 10 shows good agreement.

This case is relatively easy because prediction of wavy center defect by operator in real time is immediate. In reference [2] authors demonstrate that there are intricate situations where it is not possible to predict flatness shape based on S_{xx}^{res} measurements. The example they exposed is a case with the same boundary conditions and mesh property as well as in case 1. Geometric and mechanical parameters listed in Table 2. It is a case with lower width format and rolling tension equal to 50 MPa. Based on measured residual stress profile presented in Fig. 11 the authors found unpredictable waves in left edge, because S_{xx}^{res} is initially tensile there. This case was analyzed using numerical simulation which shows that tensile unloading begins with wavy right edge and left waves reveals at the end of the unloading. In the present work we take this example again and we note that comparison between ψ^{res} and S_{xx}^{res} gives good agreement (see Fig. 12). Our purpose is to understand the origin of unpredictable defects in such intricate cases and find correlation between residual stress measurements and flatness shape to improve flatness control.

Table 1 Case 1 data

Width b (mm)	Length a (mm)	Thickness h (mm)	Young modulus E (GPa)	Poisson ratio ν	Mesh	Tension P (MPa)
1736	8680	0.79	200	0.3	60 × 40	40

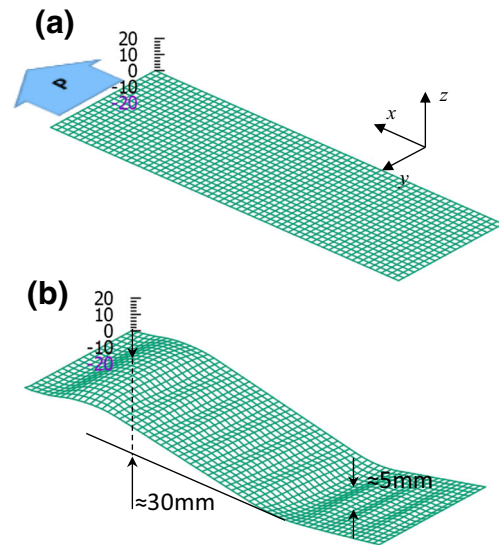


Fig. 8 Case 1: (a) Flat strip under tension, (b) wavy center defect of relaxed strip

Internal stress analysis to understand the origin of unpredictable defects

Indeed, roll sensors measure longitudinal internal stress profile $S_{xx}(y_i)$, enclosing $S_{xx}^{res}(y_i)$ and the resultant force \mathbb{F} . Only $S_{xx}^{res}(y_i) = S_{xx}(y_i) - \bar{P}$ is monitored inline, where $\bar{P} = \frac{\mathbb{F}}{hb}$. References [6–8] evoked presence of resultant moment in measurements in some cases. In Figs. 11 and 12 one sees presence of moment \mathfrak{M} of \mathbb{F} calculated as:

$$\mathfrak{M} = \int_b h y S_{xx}(y) dy \tag{10}$$

The point of application y_c of \mathbb{F} verifies the relation below:

$$\int_b h (y - y_c) S_{xx}(y) dy = 0 \tag{11}$$

In the first case \mathfrak{M} is equal to 236.84 Nm and y_c is equal to -4.78 mm. In the second case \mathfrak{M} is equal to 232.84 Nm and y_c is equal to -11.66 mm.

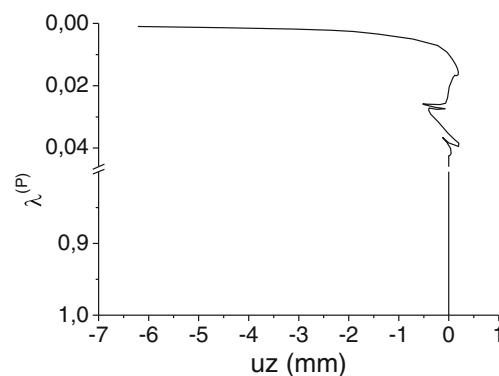


Fig. 9 Post-buckling curve of tensile unloading for case 1

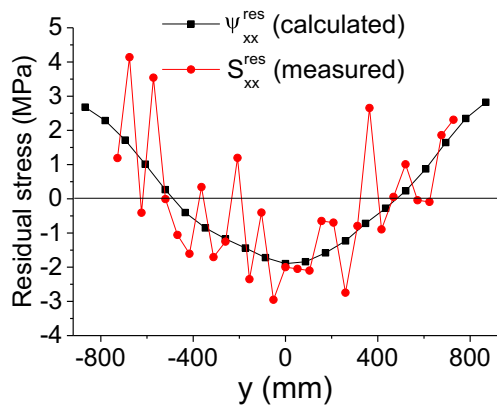


Fig. 10 Comparison between ψ_{xx}^{res} and S_{xx}^{res} for case 1

The moment \mathfrak{M} is equilibrated by coiler (or next stand). Compared to reference [2], P is used non-uniform in y -direction to apply \mathfrak{M} on border $\partial\Omega_3$ and reproduce reality. This moment is imposed as transverse gradient of longitudinal stress, therefore P is a combination between constant pressure \bar{P} (equivalent to \mathbb{F}) and non-uniform pressure $P^{\mathfrak{M}}$ (equivalent to \mathfrak{M}). The transverse shape of $P^{\mathfrak{M}}$ can have any dissymmetric form, linear for example, to give resultants \mathfrak{M} . Nevertheless, it should have the same transverse distribution as S_{xx}^{res} to minimize boundary condition perturbation due to shear stresses produced by transition (from $P^{\mathfrak{M}}(y)$ to $S_{xx}^{res}(y)$) of S_{xx} in x -direction (see Fig. 13).

According to Fig. 14a, measurements (green triangles) are interpolated on integration points (continuous black curve). Tension P is applied using $\lambda^{(P)}$ and then strip is loaded with S_{xx}^{res} using $\lambda^{(S)}$ (refer to relation (3)). Hence, longitudinal internal stress profile $S_{xx}(y)$ is calculated and represented by red circles which roll sensor detects, so in the same figure red circles coincides with curve with green triangles. If we unload P we obtain the relaxed strip state. Though, we are interested to unload only $P^{\mathfrak{M}}$ (so \mathfrak{M}) and let \bar{P} to show how the moment is transmitted into the structure. We obtain profile with blue squares showing that \mathfrak{M} has significant effect on internal stress. The difference between internal stress for strip with (red circles) and without moment (blue square) for case 2 is visualized in Fig. 14b by curve with red circles showing the contribution of \mathfrak{M} on internal longitudinal stress S_{xx} . This difference is linear in the width and attain approximately 7 MPa in edges. We conclude that resultant of P (\mathbb{F}) is transmitted in strip by its resultant and bending moment in z -direction in sense of torsor. The bending moment is identical

Table 2 Case 2 data

Width b (mm)	Length a (mm)	Thickness h (mm)	Young modulus E (GPa)	Poisson ratio ν	Mesh	Tension P (MPa)
740	8000	0.6	200	0.3	60 × 40	50

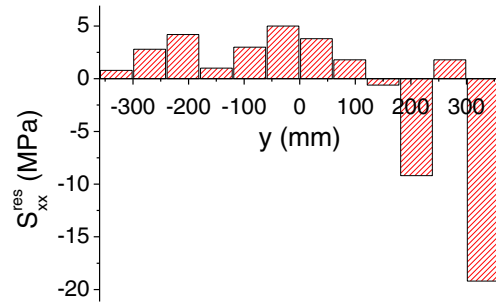


Fig. 11 Residual stress profile measured for case 2 [2]

to \mathfrak{M} and characterized by linear distribution of longitudinal stress of Fig. 14b that we note $S_{xx}^{\mathfrak{M}}(y)$. Theoretical relation between $S_{xx}^{\mathfrak{M}}(y)$ and \mathfrak{M} is deduced from Eqs. (10) and (11) as following:

$$S_{xx}^{\mathfrak{M}}(y) = \frac{12 \mathfrak{M}}{hb^3} y \tag{12}$$

We demonstrate in this section that moment unloading induces the emergence of negative residual stress at the left edge in case 2, which explain appearance of unpredictable defects there in relaxed strip.

Comments on shear stress due to the resultant moment

The presence of \mathfrak{M} induces non symmetric transverse shear stress profile S_{xy} in the strip. Fig. 15 illustrates $S_{xy}(y)$ in the middle of strip for case 2. This profile is quasi constant in x -direction and it has a resultant moment. In case 2 S_{xy} has negligible values compared with S_{xx} , even though we calculate its moment. Elementary moment applied on a portion of the strip (see Fig. 16) is dm^{xy} expressed as:

$$dm^{xy} = 2hS_{xy}dx dy \tag{13}$$

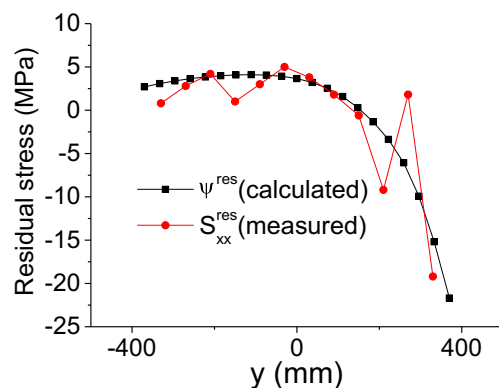


Fig. 12 Comparison between ψ_{xx}^{res} and S_{xx}^{res} for case 2

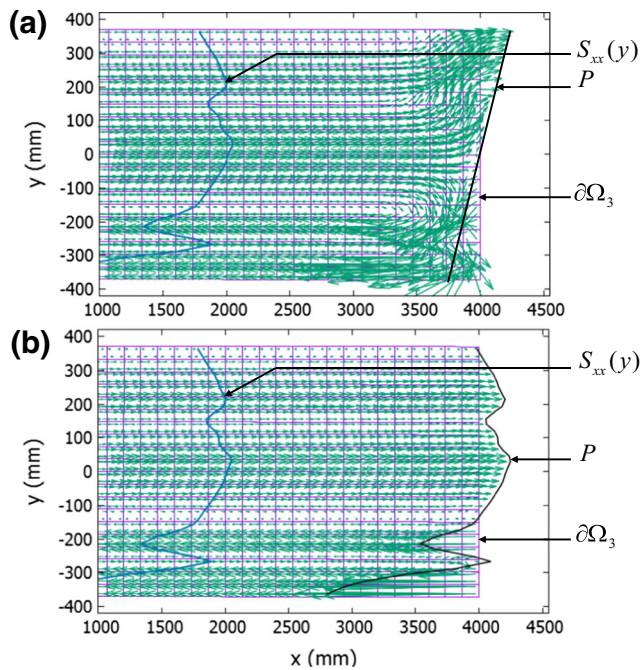


Fig. 13 Two manner of imposing tension P : (a) with linear profile, (b) with residual stress measurement profile. In plane stress field is presented by green vectors $\vec{T} = S_{xx}\vec{x} + S_{xy}\vec{y}$. In (a) we see irregular orientations of \vec{T} near to border 3 due to shear stresses. In (b) \vec{T} is almost parallel to \vec{x} because shear stresses are negligible

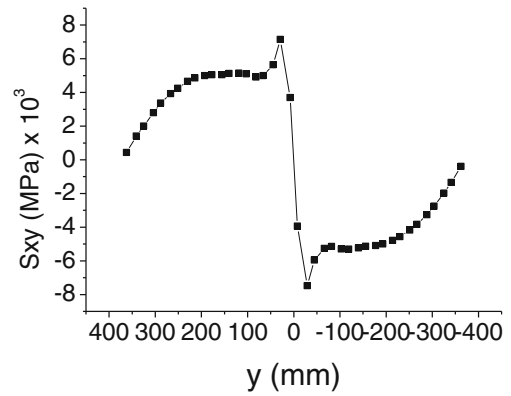


Fig. 15 Shear stress profile $S_{xy}(y)$ in the middle of the strip

This expression is integrated on the whole surface of the strip and we obtain for case 2 insignificant m^{xy} equal to 0.197 Nm.

General remark Internal stress components are almost uniform in x-direction except near to borders 1 and 3 because of boundary conditions perturbation.

A proposal for an improved residual stress measurement technique

This study proves that measurements of internal stress S_{xx} with roll sensors encloses tension resultant \bar{P} and its moment \mathfrak{M} . In this paper we propose to subtract both of these quantities from S_{xx} to deduce residual stress measurements

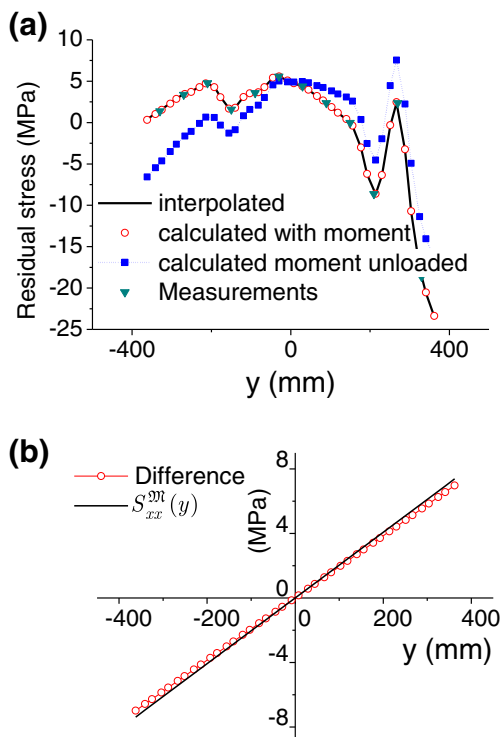


Fig. 14 a Internal stress profile with and without moment \mathfrak{M} . b Difference between internal stress profiles with and without moment \mathfrak{M}

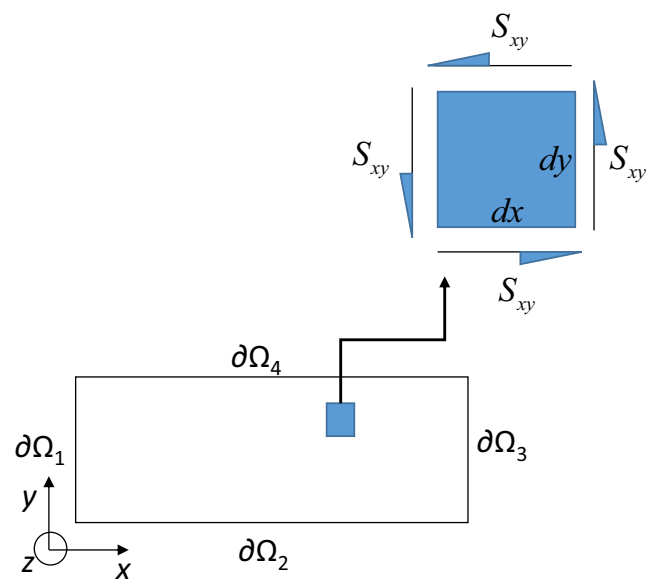


Fig. 16 Shear stress S_{xy} on a part of the strip

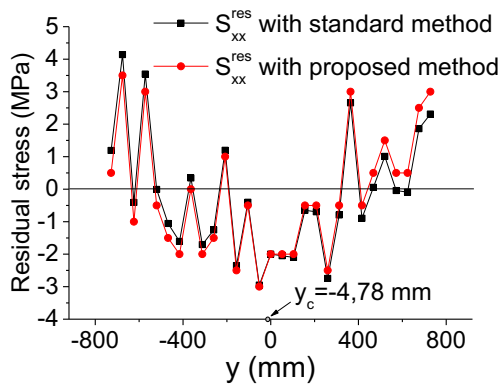


Fig. 17 Correction of residual stress measurements for case 1 using the proposed method

to predict correctly defects inline, not only \bar{P} as commonly done in industrial plants. In case 2 for example, to predict left wavy edge operator has to observe curve with blue squares instead of the one with red circles of Fig. 14a. In Figs. 17 and 18 we show the proposed measurement technique versus the usual one for respectively cases 1 and 2. In the first case the moment effect is negligible so that prediction is possible with standard method as detailed in section 3. Conversely, in the second case we should take into account resultant moment \mathfrak{M} to predict buckling in left edge since proposed method makes negative values of $S_{xx}^{res}(y)$ visible in this zone.

The same treatment is performed for ψ^{res} profile which has resultant moment equal to -156.94 Nm in case 1 and 345.23 Nm in case 2. The application point of ψ^{res} resultant force y_c is respectively 2.73 mm and -15.79 mm. When $\psi^{res}(y)$ is corrected in the same way as $S_{xx}^{res}(y)$ (elimination of both resultant $\bar{\psi}$ and its moment instead of only $\bar{\psi}$), in Figs. 19 and 20 we note that $\psi^{res}(y)$ follows $S_{xx}^{res}(y)$ changes to be in agreements with it. New residual stress expressions give negative values where flatness defects manifest.

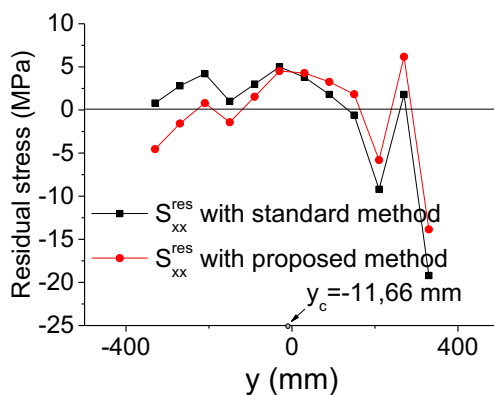


Fig. 18 Correction of residual stress measurements for case 2 using the proposed method

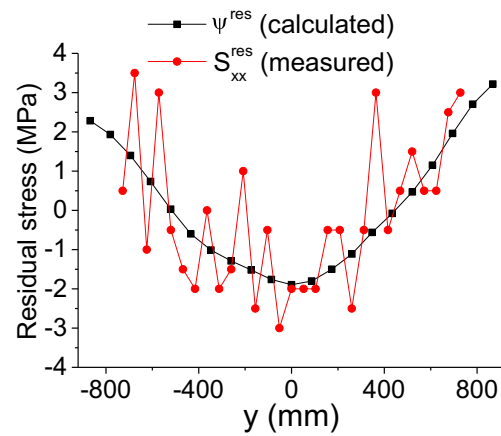


Fig. 19 Comparison between ψ^{res} and S_{xx}^{res} for case 1 using the proposed method

Conclusion

In strip rolling, measurements of residual stress field in product are provided by roll sensors placed at the outgoing of tandem mill. Note that only longitudinal component of stress fields is measured since others are neglected in this area. The residual stress profile is the main feature to evaluate in real time the strip flatness quality. In fact, because strips are fabricated under tension, geometric defects are totally or partially hidden to operator. Roll sensors measure longitudinal internal stress in strips. Conventionally resultant stress corresponding to rolling tension is subtracted to determine longitudinal residual stress profile. It is self-equilibrated and translated to I-Units according to Hooke's law in order to relate stress measurements and flatness status after tension unloading. Measurements Inline alert to defects in presence of compressive regions corresponding to positive I-Units. Operator has to maintain target residual stress profile through actuator forces to insure required flatness. However, Abdelkhalek et al. in [2] mention that in some cases defects after tension unloading appear in tensile

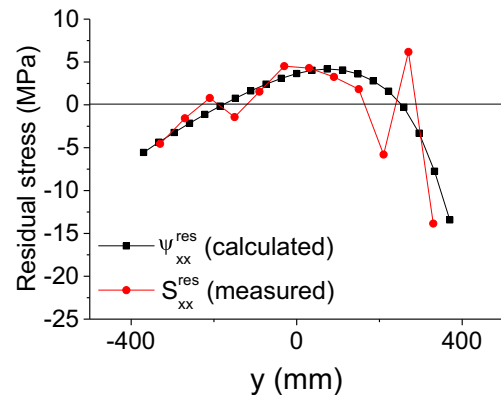


Fig. 20 Comparison between ψ^{res} and S_{xx}^{res} for case 1 using the proposal method

regions inline (negative I-Units) and this contradiction makes operator losing reference to control flatness. This study completes works of reference [2] to overcome this ambiguity. We highlight two important findings in this paper:

1. Measurements of internal stress profile contain also resultant moment with more or less significance.
2. This moment is translated into linear transverse variation of longitudinal stress and in-plane shear stress in the strip. The second is negligible.

Consequently, we propose to eliminate resultant moment profile, as well as resultant force, from internal stress measurements to rectify residual stress monitoring in real time. Examples exposed in this paper show that this improvement makes negative residual stresses visual for unpredictable defects evoked in reference [2]. Therefore, flatness defect control becomes more accurate.

Acknowledgments Author wish to thank Arcelormittal company for providing measurements and Pierre Montmitonnet for helpful and comments on the paper.

Compliance with ethical standards

Conflict of interest The authors declare that they have no conflict of interest.

References

1. Molleda J, Usamentiaga R, García D (2013) On-line flatness measurement in the steelmaking industry. *Sensors* 13(12):10245–10272. <https://doi.org/10.3390/s130810245>
2. Abdelkhalik S, Zahrouni H, Legrand N, Potier-Ferry M (2015) Post-buckling modeling for strips under tension and residual stresses using asymptotic numerical method. *Int J Mech Sci* 104:126–137. <https://doi.org/10.1016/j.ijmecsci.2015.10.011>
3. Zahrouni H, Cochelin B, Potier-Ferry M (1999) Computing finite rotations of shells by an asymptotic-numerical method. *Comput Methods Appl Mech Eng* 175(1-2):71–85. [https://doi.org/10.1016/S0045-7825\(98\)00320-X](https://doi.org/10.1016/S0045-7825(98)00320-X)
4. Büchter N, Ramm E, Roehl D (1994) Three-dimensional extension of non-linear shell formulation based on the enhanced assumed strain concept. *Int J Numer Methods Eng* 37(15):2551–2568. <https://doi.org/10.1002/nme.1620371504>
5. Boutyour EH, Zahrouni H, Potier-Ferry M, Boudi M (2004) Bifurcation points and bifurcated branches by an asymptotic numerical method and Padé approximants. *Int J Numer Methods Eng* 60(12):1987–2012. <https://doi.org/10.1002/nme.1033>
6. Kanemori S, Kinose R, Maniwa S et al (2014) Development of strip shape meter with high accuracy under severe conditions of hot strip mill. *Mitsubishi Heavy Ind Tech Rev* 51:27–31
7. Molleda J, Usamentiaga R, García DF, Bulnes FG (2010) Real-time flatness inspection of rolled products based on optical laser triangulation and three-dimensional surface reconstruction. *J Electron Imaging* 19(3):31206. <https://doi.org/10.1117/1.3455987>
8. Tsuzuki S, Yoichi K, Kenji M (2009) Flatness control system of cold rolling Process with pneumatic bearing type shape roll. *IHI Eng Rev* 42:54–60